Manufacturing and characterization of sustainable macroporous glass foams

S. K. F. da Silva[1], F. P. da Costa[1], J. V. Fernandes[1], J. B. da C. A. de Melo[2], R. R. Menezes[3],
G. de A. Neves[3], A. M. Rodrigues[3]*

[1]Federal University of Campina Grande, Graduate Program in Materials Science and Engineering,
Campina Grande, PB, Brazil
[2]Federal University of Campina Grande, Science and Technology Center,
Academic Unit of Mechanical Engineering, Campina Grande, PB, Brazil
[3]Federal University of Campina Grande, Science and Technology Center, Academic Unit of Materials
Engineering, Av. Aprígio Veloso 882, 58429-900, Campina Grande, PB, Brazil

Abstract

This work produced glass foams from soda-lime glass bottles, bentonite, and alumina by the replica method. Compositions with different contents of bentonite (5, 10, 15, and 20 wt%) were prepared and heat-treated at 800 °C. In the alumina-added compositions, 50 wt% of the bentonite was replaced by the alumina. The influences of the content of bentonite (binder) and alumina addition were evaluated through the physical-mechanical properties. The results showed that the alumina did not promote a significant effect on physical and mechanical properties in most glass foams; the exception was the sample with 20 wt% bentonite+alumina, which presented better physical properties (lower linear shrinkage and density and greater porosity) when compared to its equivalent sample (without alumina). Foams with 5% of bentonite or bentonite+alumina showed higher linear shrinkage indexes and high densification. Samples with 15% of bentonite or bentonite+alumina showed the best combination of properties: higher porosity (79.2% and 80.2%), water absorption (58.8% and 59.7%), lower shrinkage index (25.5% and 29.4%), and good flexural strength (0.69 and 0.45 MPa).
Keywords: glass foams, soda-lime glass, waste, bentonite, replica method.

INTRODUCTION

Economic development and population growth contributed to the increase in solid waste generation. Recycling reduces the number of materials sent to landfills, and glassy wastes have great potential for this process. They are 100% recyclable and can be infinitely reused depending on the circumstances. In addition, they contribute to reducing CO_2 emissions and the extraction of natural raw materials, bringing both environmental and economic benefits [1]. Due to its characteristics, several types of research have been carried out to introduce this solid waste in the manufacture of new products, such as macroporous materials [2-4]. Glass foams have a porous structure, with cells that can be isolated from each other (closed porosity) and cells that are fully or partially interconnected (open porosity) [5]. The presence of pores and their characteristics, such as size, shape, and position, in addition to their unique properties such as low density, low thermal conductivity, non-toxicity, non-flammability, chemical inertness, and low dielectric constant, enable numerous applications, such as catalysts in industry, cast metal filters, thermal or acoustic insulators, bioceramic materials, and so on [6-10].

Among the most used methods in the manufacture of glass foams, the polymeric sponge technique (replica method) stands out, which consists of a simple and low-cost manufacturing process for the formation of various types of foams, making it possible to obtain materials with greater porosity and high interconnectivity between pores [11-17]. Many types of research have been carried out involving the production of glass foams from the use of glass waste, which presents itself as an essential alternative, since, in addition to avoiding the extraction of non-renewable raw materials, it proposes an ecologically correct destination for this type of waste. Bai et al. [18] prepared glass foams from bottle glass waste and ash from a thermal plant, using SiC as a foaming agent. The analysis revealed that the increase in temperature caused a decrease in the intensity of the peaks associated with the crystalline phases mullite and cristobalite, indicating that the glass waste can react with the ash at high temperatures. The authors obtained foams with a bulk density of 267.2 kg/m^3, compressive strength of 0.9829 MPa, and porosity of 81.55%. Kavas and Kurtuluş [19] produced foams using glass waste, quartz tailings, marble powder as a foaming agent, and ulexite (boron oxide mineral) as a flux agent (1, 2, and 3 wt%). The samples were sintered at different temperatures (850 and 900 °C) and heating rates (5 and 10 °C.min^{-1}). The best results were obtained with 1 wt% of ulexite and sintered at 900 °C with a heating rate of 10 °C.min^{-1}. The foam had a density of 0.5389 g/cm^3, porosity of 67%, and thermal conductivity of 0.127 W/(m.K). Saparuddin et al.

*alisson_mendes@ymail.com
https://orcid.org/0000-0003-0449-9219

[20] developed glass-ceramic foams from soda-lime-silica glass (94 wt%) and eggshell (foaming agent) at temperatures of 700, 800, and 900 °C under a heating rate of 10 °C.min^{-1}. The analysis showed the presence of cristobalite (SiO_2) and wollastonite ($CaSiO_3$) phases. The increase in sintering temperature promoted the formation of a liquid phase that, associated with low viscosity, generated pore coalescence, and reduced linear expansion. The samples that were heated to 800 °C had a maximum porosity of 82.2%, a minimum density of 0.42 g/cm^3, and a compressive strength of 0.42 MPa. Costa et al. [21] produced glass-ceramic foams by the polymeric replica method from soda-lime glass waste and bentonite (5 vol%) as a binder. The authors analyzed the influence of glass content (30, 35, and 40 vol%) and heat treatment temperature (750, 800, and 850 °C) on the physical-mechanical properties of the foams produced. The authors managed to obtain foams with 65% porosity and flexural strength above 1 MPa. The best compromise between porosity and flexural strength was obtained for 30 vol% glass waste samples and sintered at 800 °C.

In most of the scientific works published, the authors assess the influence of temperature and sintering rate on the properties of developed foams. Thus, there is a gap in the literature regarding the influence of the binder content on the physical-mechanical properties of glass foams prepared by the polymeric replica method. Therefore, in this work, glass foams were manufactured from soda-lime glass bottles, bentonite (as a binder), and alumina by the polymeric replica method. The effects of the different bentonite contents (5, 10, 15, and 20 wt%) and alumina addition on the microstructure and physical-mechanical properties of the glass foams were evaluated.

MATERIALS AND METHODS

Materials: waste from transparent soda-lime glass bottles from domestic disposal (starting material), bentonite clay (binder) and alumina (additive, Cia. Tecnocerâmica do Brasil), sodium hexametaphosphate (dispersant, Synth, 99.5% R.G.), and polyurethane (PU) foam (Master Sponge & Foam Prod. Manufact.) with 50 ppi open-cell structure were used.

Processing and characterization of raw materials: the glass bottles were cleaned, fragmented with the aid of a hammer, and sieved (4.00 mm). The passing fraction of the waste was dry-milled for 60 min in a planetary ball mill (CT-242, Servitech) at 380 rpm. A porcelain jar containing alumina balls was used, with the proportion of 300 g of material for 12 medium (φ20 mm) and 18 small (φ10 mm) alumina balls. The same process was carried out for the alumina that was received with particle diameters above 20 μm (77% cumulative volume) and a mean diameter of 53.41 μm. The glass powder, as-received bentonite, and alumina were passed through a sieve with an opening of 74 μm. The chemical composition of the raw materials was obtained by energy dispersive X-ray spectroscopy (EDX 720, Shimadzu) in a vacuum. For this, the samples were pressed in the metal mold (20 mm diameter) at 5 tons for 30 s. For glass powder and alumina, boric acid was used as a binder. The identification

of the crystalline phases present in the raw materials was determined by X-ray diffraction analysis (XRD) using a diffractometer (D2 Phaser, Bruker) with CuKα radiation (λ=1.5418 Å), 0.02° step, and in the 2θ angle range of 5° to 60° (bentonite) and 5° to 80° (waste glass and alumina). Phase identification was obtained using Crystallographica Search-Match software. The particle size distribution was determined by the laser diffraction granulometry method (Mastersizer 2000, Malvern). The analysis was carried out in an aqueous medium, in a proportion of 250 mL of distilled water for each 5 g of material, using sodium hexametaphosphate as a dispersing agent. Thermogravimetric analysis (TGA) curves for the bentonite, alumina, and polyurethane (PU) foam were obtained using a thermal analysis system (DTG-60H, Shimadzu) in a nitrogen atmosphere and flow rate of 100 mL.min^{-1}, using a crucible of alumina at a heating rate of 10 °C.min^{-1}.

Formulation of glass foams: the formulations of the precursor aqueous suspensions of glass foams were determined based on preliminary studies by Costa et al. [1, 21]. All suspensions were prepared using the proportion of 35 vol% solids and 65 vol% distilled water. Compositions with different contents of bentonite (5, 10, 15, and 20 wt%) were prepared. In alumina compositions, 50 wt% of the bentonite was replaced by alumina. Table I summarizes the proportions of each raw material (glass, bentonite, and alumina) and the terminology used. The suspensions were homogenized in a mechanical mixer at 3600 rpm for 30 min. For all compositions, the amount of dispersant used (sodium hexametaphosphate, density 2.20 g/cm^3) was 1 vol% of the suspension.

Table I - Summary of the formulations: terminology and proportion (wt%) of glass waste, bentonite, and alumina.

Sample	Glass waste	Bentonite	Alumina
EVC 95	95	5	-
EVC 95-A	95	2.5	2.5
EVC 90	90	10	-
EVC 90-A	90	5	5
EVC 85	85	15	-
EVC 85-A	85	7.5	7.5
EVC 80	80	20	-
EVC 80-A	80	10	10

Molding, drying, and sintering of foams: the polyurethane foam samples (50x50x21 mm) were immersed in the prepared suspensions (Table I) three times with intervals of 30 min between each immersion. The excess suspension was manually removed. Drying the impregnated foams took place in two steps: first, the suds were kept at room temperature for 24 h and then dried in an oven at 110 °C for 2 h. After drying, the impregnated foams were subjected to heat treatment. Fig. 1 shows the profile of the heat treatment curve. In summary, the foams were heated up to 500 °C at a rate of 1 °C.min^{-1}, remaining

at this temperature for 30 min to eliminate the polymer matrix. Afterward, the samples were heated at 5 °C.min⁻¹ up to 800 °C, remaining at this temperature for 60 min to consolidate the structure. Cooling was carried out in three stages: cooling to 540 °C with an isothermal treatment of 30 min; followed by cooling to 440 °C for 60 min. The two steps were carried out at a cooling rate of 10 °C.min⁻¹. Finally, the samples were cooled to room temperature following the inertia of the oven.
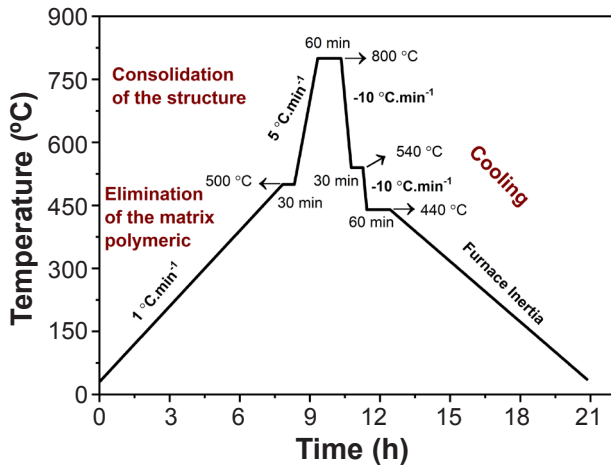

Figure 1: Thermal profile of the treatment used for the sintering of glass foams.

Physical-mechanical properties: the behavior of the foams during sintering was evaluated using the linear shrinkage (LS) determined from Eq. A. Water absorption (WA), apparent porosity (AP), and apparent density (AD) were measured using the Archimedes principle. For all measurements, a mean of eight samples was used. Before immersion in distilled water, the sintered samples were dried at 60 °C for 24 h to determine the dry weight (W_d). Then, the samples were immersed in distilled water and kept for 24 h; after this period, the wet weight (W_w) was measured. The water used for immersion of the samples was at room temperature (~25 °C). To measure the immersed weight (W_{im}), the samples were weighed on a hydrostatic analytical balance. Eqs. B, C, and D were used to calculate water absorption, apparent porosity, and apparent density, respectively:

$$LS(\%) = \frac{L_i - L_f}{L_i} .100 \qquad (A)$$

$$WA(\%) = \frac{W_w - W_d}{W_w}.100 \qquad (B)$$

$$AP(\%) = \frac{W_w - W_d}{W_w - W_{im}} .100 \qquad (C)$$

$$AD = \frac{W_w}{W_w - W_{im}} \qquad (D)$$

where L_i and L_f in Eq. A mean the length of the samples before and after sintering, respectively. The geometric density (d_G) of the foams was measured considering the mass/volume ratio. The calculation of the theoretical density (d_T) of the foams involved the theoretical density of glass (ϱ_G=2.52 g.cm⁻³), bentonite (ϱ_B=0.95 g.cm⁻³), and alumina (ϱ_A=3.95 g.cm⁻³) and was calculated according to Eq. E. The geometric and theoretical densities of the foams were used to calculate the total porosity (P_T) by Eq. F and closed porosity (P_C) was calculated by Eq. G:

$$d_T = \%glass.\rho_G + \%bentonite.\rho_B + \%alumina.\rho_A \quad (E)$$

$$P_T (\%) = 1 - \frac{d_G}{d_T} \qquad (F)$$

$$P_C (\%) = P_T - AP \qquad (G)$$

The mean pore size of each composition was obtained from pore measurements from three optical micrograph images. The mechanical properties of the foams were measured using the three-point flexural test, with the aid of a universal testing machine (AG-X 50kN, Shimadzu), with a load cell of 5 kN, the distance between the support points of 30 mm, and speed of 0.5 mm.min⁻¹. Eight samples (50x10x5 mm) were used for each composition. The test was carried out at room temperature (~28 °C). The flexural tensile stress (σ_f in MPa) was calculated using Eq. H:

$$\sigma_f = \frac{3.L.D}{2.b.h^2} \qquad (H)$$

where L is the applied load (N), D is the distance between supports (mm), b and h are the horizontal dimension and height of the specimen (mm), respectively.

RESULTS AND DISCUSSION

Characterization of raw materials: the chemical composition of the raw materials used in the manufacture of foams is shown in Table II. The glass waste was predominantly formed by silicon oxide - SiO_2 (69.6%),

Table II - Chemical composition (wt%) of raw materials.

Raw material	SiO_2	CaO	Na_2O	Al_2O_3	K_2O	Fe_2O_3	TiO_2	MgO	Others
Glass waste	69.6	12.9	11.9	3.79	0.91	-	0.06	-	0.84
Bentonite	64.6	2.27	-	18.2	1.12	9.47	1.03	2.75	0.54
Alumina	0.50	0.06	-	99.4	-	0.03	-	-	-

sodium oxide - Na_2O (11.9%), and calcium oxide - CaO (12.9%), characteristic of soda-lime glass. Al_2O_3 (3.79%), TiO_2 (0.06%), and K_2O (0.91%) were also detected in the glass waste. The bentonite showed SiO_2 (64.6 wt%) and alumina - Al_2O_3 (18.2 wt%) as major oxides. A high content of Fe_2O_3 (9.47 wt%) was also identified in bentonite. SiO_2 and Al_2O_3 were combined, for the most part, to form clay minerals [22]. The presence of a high concentration of Fe_2O_3 contributes to lowering the dehydroxylation temperature. The contents of MgO (2.75 wt%) and CaO (2.27 wt%) confirmed its polycationic nature. The values for the other oxides were within the expected range for bentonite clays [23-25]. Alumina had 99.4% Al_2O_3, and traces of SiO_2, CaO, and Fe_2O_3 were possible impurities impregnated during processing.

Fig. 2 shows the X-ray diffractograms of the glass waste, bentonite, and alumina. The glass waste (Fig. 2a) presented only a broad band between 14° and 40° (2θ) characteristic of silica-based glasses. The absence of crystalline peaks is the main characteristic of vitreous materials. The diffractogram obtained from bentonite (Fig. 2b) showed the predominant presence of clay mineral montmorillonite - $AlSi_2O_6(OH)_2$ (PDF 00-002-0037), kaolinite - $Al_4(OH)_8Si_4O_{10}$, (PDF 01-078-2110), and quartz - SiO_2 (PDF 00-012-0708). It was also observed the significant presence of accessory minerals such as palygorskite - $(Mg,Al)_5(Si,Al)_8O_{20}(OH)_{28}H_2O$ (PDF 00-021-0958) and cristobalite - SiO_2 (PDF 00-039-1425). The bentonite also showed the presence of a trace of calcite - $CaCO_3$ (PDF 00-005-0586). In the alumina XRD pattern (Fig. 2c), the presence of corundum - α-Al_2O_3 (PDF 00-046-1212) was the predominant crystalline phase since it is the most stable form at all temperatures. Peaks of aluminum oxide - Al_2O_3 phase (PDF 00-031-0026) were also detected in the alumina.

Fig. 3 shows the particle size distribution curves (cumulative and frequency) for glass waste after the grinding process, bentonite, and alumina. The glass waste (Fig. 3a) was constituted by a set of particles smaller than 150 μm, with D_{10}=2.79 μm, D_{50}=25.05 μm, and D_{90}=66.26 μm. The frequency curve exhibited a monomodal distribution, with the peak at 44.69 μm and a narrower curve profile, indicating greater uniformity in particle size. Bentonite (Fig. 3b) was formed by smaller particles (<40 μm), when compared to waste glass (<150 μm), with values of D_{10}=0.93 μm, D_{50}=4.22 μm, and D_{90}=13.86 μm. The frequency curve presented a monomodal profile with a peak at 4.86 μm. On the other hand, the alumina frequency curve (Fig. 3c) showed a bimodal distribution, with two peaks at 1.74 and 23.54 μm and with 100% of the total distribution below 90 μm. Compared to waste glass, alumina had a wider curve profile, with considerable variation in particle size. The values for D_{10}, D_{50}, and D_{90} obtained from the cumulative alumina curve were 0.98, 4.66, and 34.59 μm, respectively.

The study of the thermal behavior of the raw materials used and the polyurethane foam was of fundamental importance. Due to this thermal study, it was possible to know the different characteristics of the raw materials
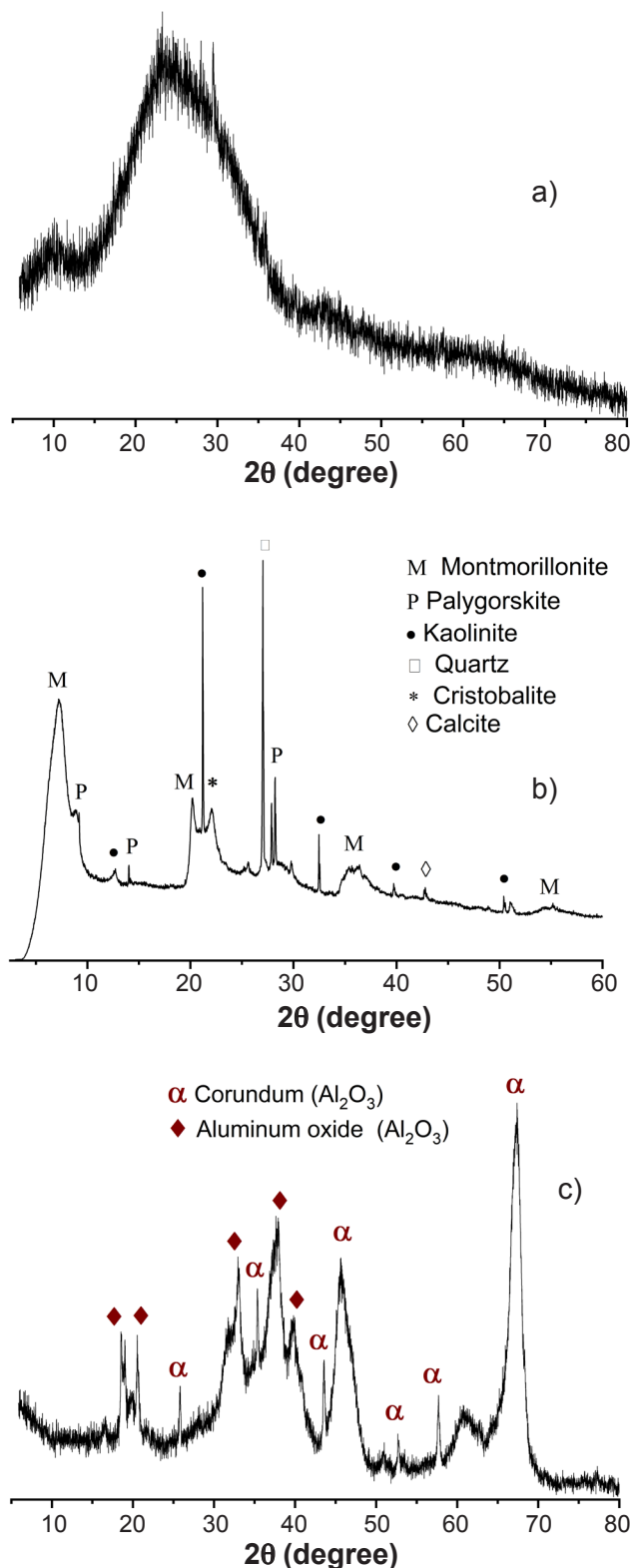
Figure 2: X-ray diffractograms of glass waste (a), bentonite (b), and alumina (c).

as a function of the temperature. Fig. 4 shows the thermogravimetric analysis (TGA) and its derivative (DTG) curves for bentonite, polyurethane foam, and alumina, displaying the main thermal events that took place during the heating of the samples at a heating rate of 10 ºC.min^{-1}
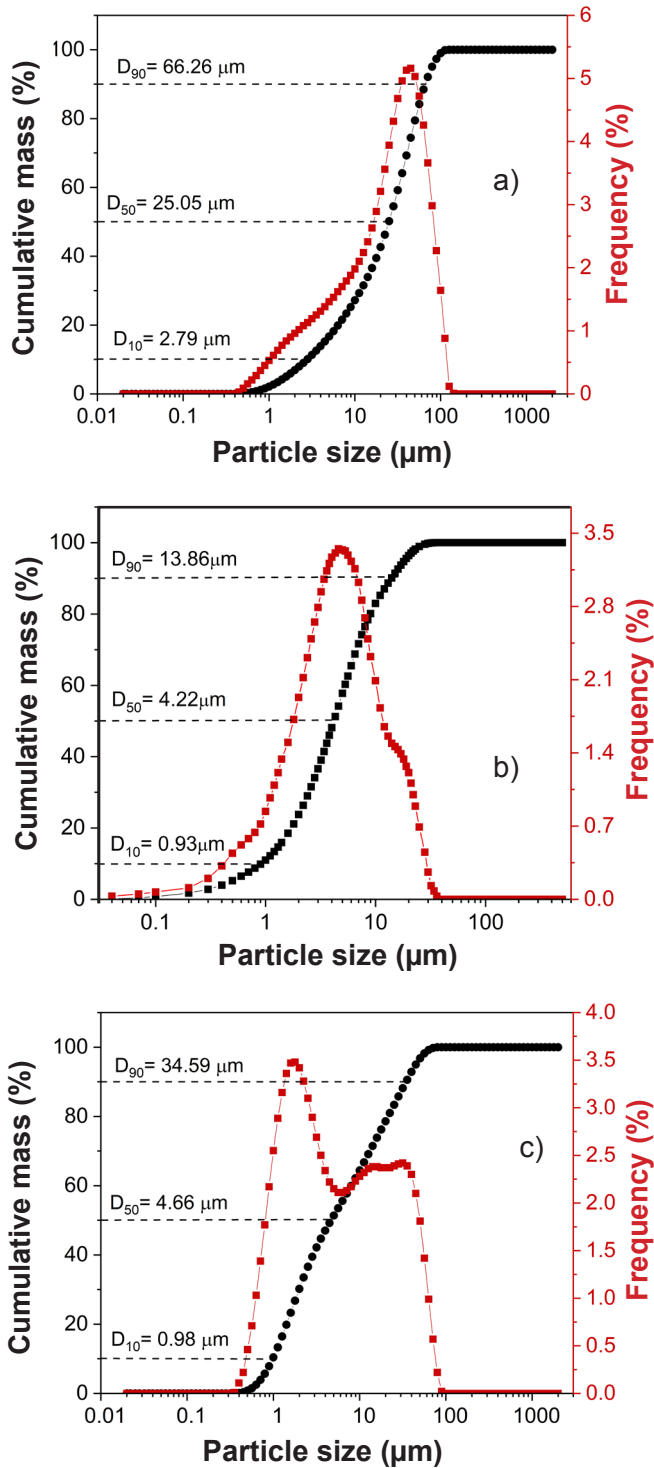
Figure 3: Particle size distribution curves of glass waste (a), bentonite (b), and alumina (c).

from room temperature (~27 °C) to 850 °C. Bentonite (Fig. 4a) presented three stages of mass loss. The first, with 11.9% of mass loss, occurred in the temperature range between 25 and 179 °C and was associated with the elimination of water between the layers (free water), which usually occurs at temperatures below 200 °C. Between 179 and 566 °C, there was a 4.8% mass loss due to the loss of hydroxyl groups from the structure of clay minerals and the elimination of organic

matter [26]. The third and last mass loss (1.7%) occurred between 566 and 850 °C. This loss can be attributed to the decomposition of calcite present in bentonite (Fig. 2b) into oxides ($CaCO_3 \rightarrow CaO + CO_2$) [27]. The total mass loss of bentonite was 18.4%. The polyurethane foam showed 100% mass loss up to the temperature of ~550 °C, and its degradation occurred in two stages (Fig. 4b). The first occurred in the temperature range between 31 and 312 °C with a mass loss of 48.6%, and the second occurred between 312 and 551 °C
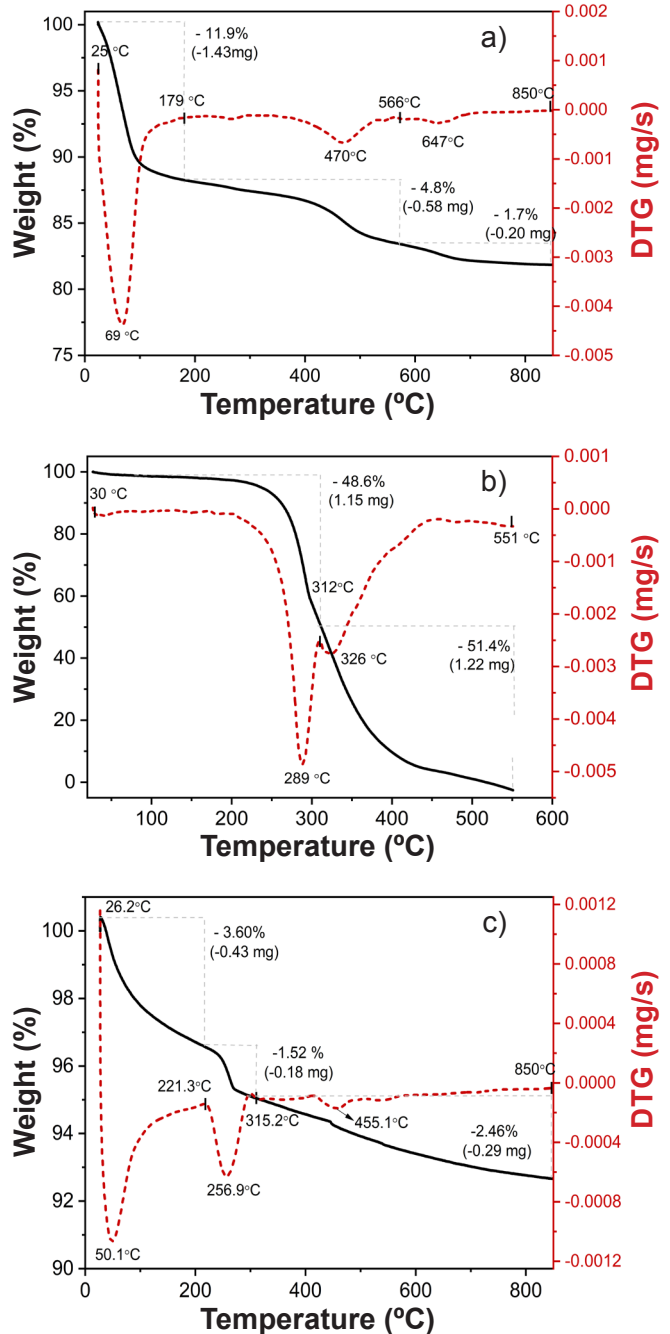

Figure 4: Curves of thermogravimetric analysis (TGA) and its derivative (DTG) of bentonite (a), polyurethane foam (b), and alumina (c), obtained with a heating rate of 10 °C.min^{-1} in a nitrogen atmosphere.

with a mass loss of 51.4%. These mass loss values were associated with the decomposition products CO_2, CO, NH_3, and isocyanides [28, 29]. Thus, it was necessary that, in this range of polyurethane degradation, the heating rate was slow to ensure total foam volatilization without damaging the ceramic foam structure. Alumina (Fig. 4c) presented two main thermal events. The first, between 26 to 221 °C with approximately 3.6% loss, was caused by the elimination of water. The second thermal event can be attributed to the decomposition of aluminum hydroxide [30]. In this stage, two endothermic peaks were observed from the DTG curve, indicating the evolution of the decomposition process in two steps. The first step occurred between 221 and 315 °C with 1.5% of mass loss and the second was between 315 and 850 °C, with a loss of 2.5%. The total loss of alumina was 7.6%.

Physical and mechanical properties of glass foams: Figs. 5a to 5d show, respectively, the results obtained for linear shrinkage (LS), apparent (AD) and geometric (d_G) density, porosity (AP), and water absorption (WA) of the glass foams sintered at 800 °C. Samples with 5 and 20 wt% of bentonite and 5 wt% of bentonite+alumina (EVC 95, EVC 80, and EVC 95-A) showed higher LS values (37.4%, 39.8%, and 40.4%, respectively, Fig. 5a). In relation to the EVC 95-A and EVC 95 glass foams, such behavior can be due to the high soda-lime glass content; therefore, a larger relative liquid phase was formed, which filled the internal pores. On the other hand, the higher LS value measured for the EVC 80 glass foam can be explained due to the higher relative amount of bentonite in this composition. The bentonite used in this work presented high Fe_2O_3 content (9.47 wt%). Indeed, Fe_2O_3 is known as fluxing agent; thus, a greater amount of liquid phase was formed during the thermal treatment that filled the pores [31]. Therefore, the more pores filled, the more densified and less porous the samples are (Figs. 5b and 5c). In general, it was not observed significative effect of Al_2O_3 on the LS values for glass foams containing the same glass contents; for example, the LS values for the EVC 90-A and EVC 90 glass foams were 29.1% and 28.0%, respectively. The same behavior was observed for apparent and geometric density, porosity, and water absorption (Figs. 5b to 5d). Al_2O_3 was added for the glass foam compositions aiming to control the shrinkage and porosity; however, the effect of the Fe_2O_3 as the fluxing agent was predominant. The exception was observed for the EVC 80-A glass foam, which had the highest Al_2O_3 content (10 wt%) and presented a 31.2% reduction in linear shrinkage and a 45.1% increase in total porosity when compared to EVC 80 (without alumina). Fig. 5c shows that open porosity was predominant in all samples. Such behavior is the advantage of the sacrificial element using polyurethane foams which had a large set of open cells (50 ppi in this work). Due to more significant shrinkage, the samples EVC 95, EVC 95-A, and EVC 80 had lower total porosity (46.0%, 40.6%, and 52.1%) and absorbed less water (21.1%, 16.1%, and 29.6%) compared to the others (AP between 70.8%-80.2%; WA between 50.2%-59.7%). Samples EVC 85 and EVC 85-A had the highest total porosity values, with 79.1% and 80.2%
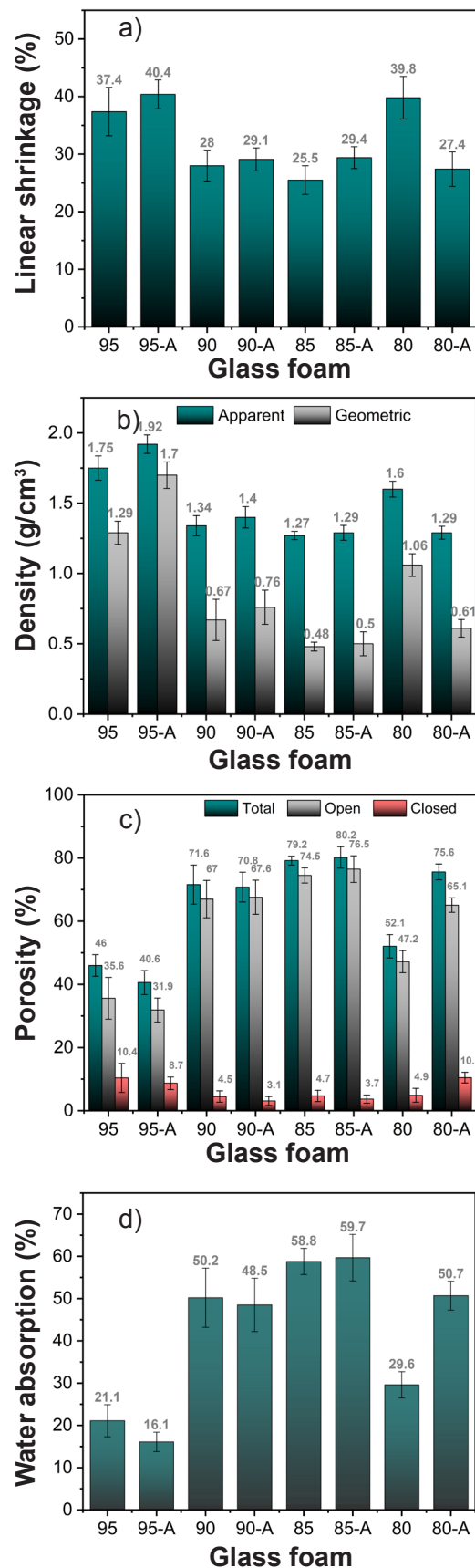

Figure 5: Physical properties of glass foams: a) linear shrinkage; b) apparent and geometric density; c) porosity; and d) water absorption.

These values were higher than those (63%-75%) found by Costa et al. [1].

Table III shows the results of the flexural strength and average pore diameter of glass foams. The foams with the lowest bentonite and bentonite+alumina contents (5 wt%) had the highest values of flexural strength: 2.80 ± 1.03 and 3.34 ± 0.58 MPa for EVC 95 and EVC 95-A, respectively. A significant decrease in flexural strength (between 75.4% and 91.4%) was observed with the increasing amount of bentonite for contents above 5 wt%. This behavior was related to the higher porosity values presented by the compositions with bentonite content above 5 wt%. This result was already expected because the pores act as stress concentrators, accelerating the initiation and propagation of internal cracks, leading to material fracture. This behavior is related to the greater densification of EVC 95 and EVC 95-A foams during the thermal treatment, resulting in thicker cell walls. Thicker cell walls increase the effective load-bearing area and, consequently, the flexural strength [1]. The insertion of alumina also did not significantly affect the flexural strength of the glass foams. In general, the glass foams had a mean pore diameter between 269 and 417 μm. It was observed that the average pore diameter increased with an increasing amount of bentonite. This behavior may be related to pore filling by the viscous phase, corroborating the results of physical properties (Fig. 5).

Table III - Flexural strength and average pore diameter of glass foams.

Sample	Flexural strength (MPa)	Average pore diameter (μm)
EVC 95	2.80 ± 1.03	353 ± 107
EVC 95-A	3.34 ± 0.58	298 ± 98
EVC 90	0.38 ± 0.16	320 ± 118
EVC 90-A	0.44 ± 0.18	269 ± 89
EVC 85	0.69 ± 0.18	383 ± 144
EVC 85-A	0.45 ± 0.18	322 ± 109
EVC 80	0.58 ± 0.30	417 ± 135
EVC 80-A	0.37 ± 0.05	413 ± 111

Morphological characterization of foams: Fig. 6 shows images acquired from glass foams prepared with different bentonite and bentonite+alumina contents (5, 10, 15, and 20 wt%) and PU foam used as a mold. It was possible to observe that all the foams developed presented macropores (>0.05 μm) [7] compatible with those of the PU foam used as a replica. The samples EVC 80, EVC 85, and EVC 90 showed a more reddish color. This characteristic was related to the higher concentration of bentonite clay in their formulations (20, 15, and 10 wt%), which was rich in Fe_2O_3, a flux oxide of high pigmentation. It was also possible to observe in the foams with a lower content (5 wt%) of bentonite/bentonite+alumina (EVC 95 and EVC 95-A) a glassy layer formation along the edges. Furthermore, it can
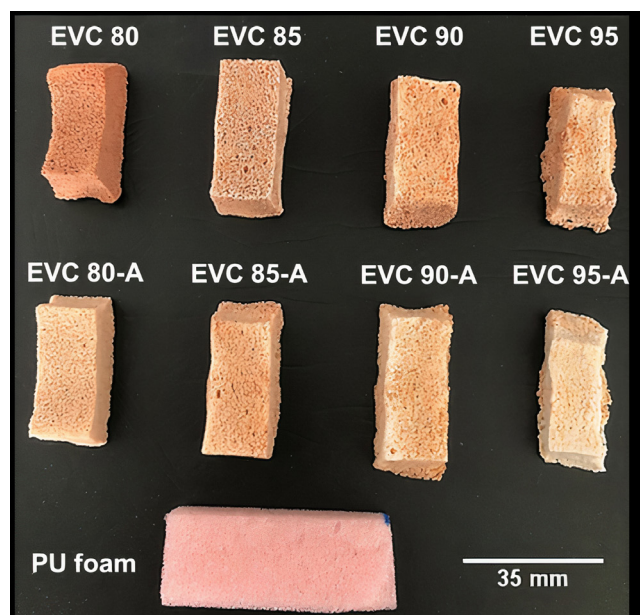

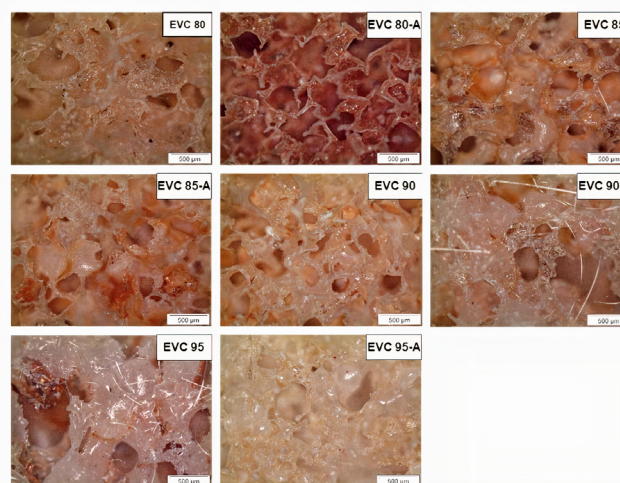Figure 6: Image showing the PU and glass foams.

Figure 7: Optical micrographs obtained from the surface of the glass foams.

be clearly seen that EVC 80, EVC 95, and EVC 95-A glass foams were the ones that shrank the most, corroborating the linear shrinkage data (Fig. 5a). Fig. 7 shows the optical micrographs of the surface of the glass foams. It was noticeable that EVC 95 and EVC 95-A foams had denser walls due to the higher proportion of vitreous waste that increased the system's viscosity, facilitating the filling of internal pores. Thicker cell walls increased the flexural strength of these glass foams, as shown in Table III.

CONCLUSIONS

Several glass foam compositions were successfully manufactured from soda-lime bottle waste, bentonite, and alumina using the polymeric replica method. The bentonite clay used as a binder contributed to the liquid phase formation, fundamental for the densification and structuring of the samples. In addition, it conferred foams of a reddish

color. Alumina did not promote a significant effect on physical and mechanical properties in most glass foams; the exception was the EVC 80-A sample (80 wt% glass and 20 wt% bentonite+alumina) which presented a 31.2% reduction in linear shrinkage and a 45.1% increase in total porosity when compared to sample without alumina (EVC 80). The EVC 95 (5 wt% of bentonite), EVC 95-A (5 wt% of bentonite+alumina), and EVC 80 (20 wt% of bentonite) glass foams had a more significant shrinkage during thermal treatment (37.4%, 40.4%, and 39.8%) and greater density values (1.75, 1.92, and 1.60 g/cm^3). Samples EVC 85 and EVC 85-A (15 wt% bentonite/bentonite+alumina) presented the best set of properties: higher porosity (79.2% and 80.2%), water absorption (58.8% and 59.7%), less shrinkage index (25.5% and 29.4%), and good flexural strength (0.69±0.18 and 0.45±0.18 MPa).

ACKNOWLEDGMENTS

REFERENCES

[1] F.P. da Costa, C.R.S. Morais, H.C. Pinto, A.M. Rodrigues, Mater. Chem. Phys. **256** (2020) 123612.

[2] N.P. Stochero, J.O.R.S. Chami, M.T. Souza, E.G. de Moraes, A.P.N. de Oliveira, Waste Biomass Valorization **12**, 3 (2021) 1609.

[3] L.F. Jochem, C.A. Casagrande, L. Onghero, C. Venâncio, P.J.P. Gleize, Constr. Build. Mater. **273** (2021) 121704.

[4] D. Kazmi, M. Serati, D.J. Williams, S. Qasim, Y.P. Cheng, J. Clean. Prod. **284** (2021) 124762.

[5] J. Luyten, S. Mullens, J. Cooymans, A.M. De Wilde, I. Thijs, R. Kemps, J. Eur. Ceram. Soc. **29** (2009) 829.

[6] M. Scheffler, P. Colombo, *Cellular ceramics: structure, manufacturing, properties and applications*, Wiley-VCH, Weinheim (2006).

[7] A.V. Santos, M.M. Viana, F.H.A. Medeiros, N.D.S. Mohallem, Quím. Nov. **38**, 1 (2016) 4.

[8] I. Bernardo, E. Castellan, R. Hreglich, S. Lancellotti, J. Eur. Ceram. Soc. **26**, 15 (2006) 3335.

[9] M. Zhu, R. Ji, Z. Li, H. Wang, L. Liu, Z. Zhang, Constr. Build. Mater. **112** (2016) 398.

[10] W. Guo, H. Li, F. Ye, Ceram. Int. **42**, 15 (2016) 17332.

[11] Z. Švagelj, L. Ćurković, V. Mandić, V. Rede, in 9th Int. Sci. Expert Conf. TEAM, Novi Sad (2018) 110.

[12] C. Yagsi, O. Keles, Miner. Met. Mater. Ser. **30** (2019) 209.

[13] N.S. Suparman, K.A. Alwi, M.A.A.M. Nor, Mater. Sci. Forum **840** (2016) 77.

[14] S. Karimi, T. Go, R. Vaßen, J. Gonzalez-Julian, Mater. Lett. **240** (2019) 271.

[15] R. Muda, M.A. Azmi, S. Mahzan, H.M. Elwalwal, S. Ahmad, H. Taib, Key Eng. Mater. **791** (2018) 37.

[16] M. Araújo, R. Viveiros, A. Philippart, M. Miola, S. Doumett, G. Baldi, J. Perez, A.R. Boccaccini, A. Aguiar-Ricardo, E. Verné, Mater. Sci. Eng. C **77** (2017) 342.

[17] M.S. Sharmiwati, R.M. Mizan, A.B. Noorhelinahani, Int. J. Sci. Technol. Res. **3**, 6 (2014).

[18] J. Bai, X. Yang, S. Xu, W. Jing, J. Yang, Mater. Lett. **136** (2014) 52.

[19] T. Kavas, R. Kurtuluş, in 20th Int. Symp. Boron, Borides & Related Mater., Niigata (2019).

[20] D.I. Saparuddin, N.A.N. Hisham, S. Ab Aziz, K.A. Matori, S. Honda, Y. Iwamoto, M.H.M. Zaid, J. Mater. Res. Technol. **9**, 3 (2020) 5640.

[21] F.P. da Costa, C.R.S. Morais, A.M. Rodrigues, Ceram. Int. **46** (2020) 17957.

[22] S.C. Taylor-Lange, E.L. Lamon, K.A. Riding, M.C.G. Juenger, Appl. Clay Sci. **108** (2015) 84.

[23] L.N. Santana, J. Gomes, G. Neves, H.L. Lira, R.R. Menezes, A.M. Segadães, Appl. Clay Sci. **87** (2014) 28.

[24] I.A. Silva, J.M.R. Costa, R.R. Menezes, H.S. Ferreira, G.A. Neves, H.C. Ferreira, Rev. Esc. Minas. **66** (2013) 485.

[25] I.C.G. Morais, I.A. Silva, B.M.A.B. Buriti, J.V. Fernandes, D.S. Silva, G.A. Neves, H.S. Ferreira, Cerâmica **66**, 377 (2020) 81.

[26] M.V. Kok, Energy Sources **24**, 10 (2002) 907.

[27] J.F. Duarte Neto, I.D.S. Pereira, V.C. da Silva, H.C. Ferreira, G. de A. Neves, R.R. Menezes, Cerâmica **64**, 372 (2018) 598.

[28] M. Herrera, M. Wilhelm, G. Matuschek, A. Kettrup, J. Anal. Appl. Pyrolysis **58** (2001) 173.

[29] E. Sousa, C.B. Silveira, T. Fey, P. Greil, D. Hotza, A.P.N. de Oliveira, Adv. Appl. Ceram. **104** (2005) 22.

[30] S.M. Safwat, M.E. Matta, J. Dispers. Sci. Technol. **39**, 12 (2018) 1699.

[31] Y. Chi, J. Lin, B. Xu, Glas. Phys. Chem. **45**, 2 (2019) 104.

.